İSTANBUL UNIVERSITY CERRAHPAŞA

ORIGINAL ARTICLE
Electrica 2024; 24(3): 780-788

A 10-W GaN on SiC CPW MMIC High-Power Amplifier With 44.53% PAE for X-Band AESA Radar Applications

Galip Orkun Arıcan, Burak Alptuğ Yılmaz

ASELSAN Inc., Communication and Information Technologies Division, Ankara, Türkiye

Cite this article as: G. O. Arıcan and B. A. Yılmaz, "A 10-W GaN on SiC CPW MMIC high power amplifier with 44.53% PAE for X-band AESA radar applications," *Electrica*, 24(3), 780-788, 2024.

ABSTRACT

This article presents a novel X-band gallium nitride (GaN) on silicon carbide (SiC) co-planar waveguide (CPW) monolithic microwave integrated circuit (MMIC) high-power amplifier (HPA) design for radar applications. In design, 0.25 μm γ-shape gate and high electron mobility transistors (HEMTs) with GaN on SiC technologies were utilized due to their high thermal conductivity and high-power handling capability. In addition, the reflection coefficients were below −10 dB in the frequency range from 8.5 GHz to 10.5 GHz which yields a fractional bandwidth of 21.05%. Moreover, MMIC HPA achieved a power-added efficiency (PAE) of 44.53% with an output power of 40.06 dBm in the 2 GHz bandwidth. Furthermore, the proposed MMIC HPA could be appropriate to be utilized in X-band active electronically scanned array radar applications owing to its high output power, wide operating bandwidth, high PAE, and compact size.

Index Terms—Active electronically scanned array (AESA) radar, co-planar waveguide (CPW), gallium nitride (GaN) on silicon carbide (SiC), high electron mobility transistor (HEMT), monolithic microwave integrated circuit (MMIC), high power amplifier (HPA).

I. INTRODUCTION

According to the latest trends and emerging technologies, naval, land, and aerospace platforms need to be smaller, compact, long-range, and wideband active electronically scanned array (AESA) radars with a large number of active elements to catch up with technological developments [1, 2]. A number of transmitter blocks, more than thousand in general, have been used in AESA radars, and deployment of them in relatively small areas is creating thermal problems which could be solved by utilizing highly efficient high-power amplifiers (HPAs). They are extensively utilized in X-band radar applications because of not solely their high efficiency and high-power output characteristic but also their neat structures. Additionally, Gallium Nitride (GaN) on Silicon Carbide (SiC) monolithic microwave integrated circuit (MMIC) technology is preferred in the design and fabrication of HPAs instead of conventional Si-based technology. Therefore, they could operate at relatively higher temperatures than amplifiers that are fabricated by utilizing other technologies such as Gallium Arsenide (GaAs), Indium Phosphate (InP), Silicon Germanium (SiGe), Silicon (Si) etc. [3-5]. Furthermore, HEMTs have been preferred in MMICs because they have high breakdown voltage and high electron velocity, which is advantageous with respect to GaAs and Si MMIC technology [6, 7]. It is an approximate guide that compact amplifiers with high output power are the reason for preference in modern AESA radars to perform tracking and searching operations in long ranges with small platforms for reducing radar cross section (RCS). Finally, by integration of the proposed HPA with filtennas that work as a filter to reject undesirable or threatening frequency bands [8, 9], the whole system will be suitable for Electronic Counter Counter-Measures (ECCM) operations because Frequency Hopping Spread Spectrum (FHSS) requirement could be required wideband HPAs [10, 11].

In this article, a novel X-band HPA design utilizing GaN on SiC co-planar waveguide (CPW) MMIC for radar applications was presented. In addition, the details of the design and the comparison of the electromagnetic (EM) simulation results of the design and measurement results of the fabricated MMIC HPA were also given. The proposed MMIC HPA achieved a power-added efficiency (PAE) of 44.53% with an output power of 40.06 dBm in the 2 GHz bandwidth. Moreover, the reflection coefficients were below −10 dB in the frequency range from 8.5 GHz to 10.5 GHz which yields

Corresponding author:
Galip Orkun Arıcan

E-mail:
goarican@aselsan.com

Received: July 12, 2024

Revision Requested: September 20, 2024

Last Revision Received: September 24, 2024

Accepted: September 30, 2024

Publication Date: October 30, 2024

DOI: 10.5152/electrica.2024.24090

a fractional bandwidth of 21.05%. The proposed MMIC HPA comes up with enhancements for thermal problems, size, power consumption, and operational bandwidth of AESA radars. For the case of stability and high-power gain, a parallel connected capacitor and resistor structure and 0.25 μm γ-shape gate technology were utilized in fabrication, respectively. It is important to specify that HEMTs with GaN on SiC technology have been utilized in MMICs. This technology has been favored because of its high thermal conductivity and high-power handling capability. The device is well suited for AESA radars because of its high output power, wide operating frequency, high PAE, and small size. Because of the presented enhancements, it is a good nominee for AESA radars in accordance with the literature survey [12-21], and it could be directly turned to account in communication, electronic warfare, and satellite applications. Meanwhile, the design has a compact size of 5 mm × 6.5 mm (approximately 0.16 λ × 0.2 λ at 9.5 GHz). As a result, simulations were performed with Keysight Advanced Design System (ADS) and small and large signal parameters of the device have been analyzed in Sections 3 and 4 in depth. Moreover, measurements were done in a cleanroom with using a power network analyzer (PNA), spectrum analyzer (SA), and load–pull system (LPS). After measurement results are examined and checked against simulation results, possible measurement errors and differences are commented.

II. GAN ON SIC FABRICATION PROCESS

Design and fabrication of the proposed MMIC HPA were performed in Nanotechnology Research Center, Bilkent University, Türkiye. In this technology, the 300 nm GaN epitaxial layer growth was implemented on 300 μm SiC substrate, and the dielectric constant of the substrate was achieved 9.8 at 300° Kelvin. The heterostructure of the active components was grown by utilizing metal organic chemical vapor deposition (MOCVD) on SiC by the virtue of having the high thermal conductivity characteristic of SiC. Additionally, the mesa etch process was utilized to accomplish the isolation between the active components with the formation of Ti/Al/Ni/Au multilayer ohmic contacts 120/1200/350/650 Å, respectively. Meanwhile, the γ-shaped gate was developed by utilizing e-beam lithography with a gate length of 250 nm. Moreover, four metallization layers, which are 1st metal, 2nd metal, nickel chrome (NiCr) resistance, and air bridge, were utilized in the the GaN on SiC fabrication process. Additionally, NiCr thin film resistance, which has a sheet resistance of 20 Ω/square, was growth in the e-beam evaporator. 1st metal, 2nd metal, and air bridge were formed of 3 μm Au and NiCr resistance metal was formed of 1 μm NiCr material. Furthermore, the passivation layer of the silicon nitride (SiN) passivation layer, which has a thickness of 300 nm, was deposited by utilizing plasma-enhanced chemical vapor deposition (PECVD). The physics of GaN on SiC MMIC HPA is shown exhaustively in Fig. 1.

III. DESIGN

In the design, it was aimed to obtain an MMIC HPA that can be operated in the X-band (8.5 GHz to 10.5 GHz) with an output power above 40 dBm and power added efficiency (PAE) above 43%. So as to achieve the goals of the design, SiC on GaN process technology of the Nanotechnology Research Center was utilized. In addition, CPW design topology, which has signal strips and ground planes in the same side of the substrate, was utilized in the design to decrease the manufacturing cost and eliminate the complex via-hole process. In the selection of the unit transistor, a variety of different-sized HEMTs were characterized and on-wafer S-parameters and load–pull measurements were carried out to determine the best periphery for the design. As a result of the transistor analyses, 6 fingers by 125 μm unit cell was selected as the unit cell in compliance with small signal gain, output power, and PAE. Moreover, the on-wafer load–pull measurements of the 6 × 125 μm transistor were performed with the Maury load–pull system, and optimum load and source impedances for the center frequency were determined as (9.4+j×24.7) Ω and (35.1+j×13.6) Ω, respectively. Furthermore, the quiescent bias point of the unit transistor was chosen at class AB with the drain voltage (V_{ds}) of 28 V and the drain current (I_{ds}) of 175 mA, respectively. The general block diagram of the device is shown in Fig. 2. In the design, two identical MMIC HPAs were determined to deploy in parallel via two-way Wilkinson power dividers (WPDs) to multiply output power by 2.

The schematic view of HPA is shown in Fig. 3. The utility of elements was explained respectively from left to right (from Port 1 to Port 2) with respect to the schematic view except for elements that have the same duty in circuitry. In addition, the input and output matching networks (IMN & OMN) were designed to match the unit transistor to the complex conjugates of the selected load and source impedances. In the design, the gate and drain biases were supplied on the spiral choke inductors (L1, L2, L3, and L4), which were designed as high impedance to ensure the isolation between the RF and DC, and shunt capacitors (C6, C10, C16, and C20) to block the RF signal and

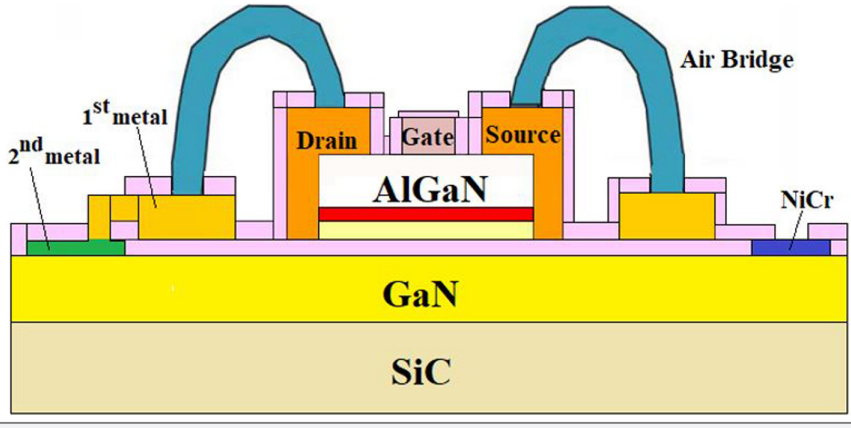

Fig. 1. Physics of GaN on SiC MMIC tehnology.

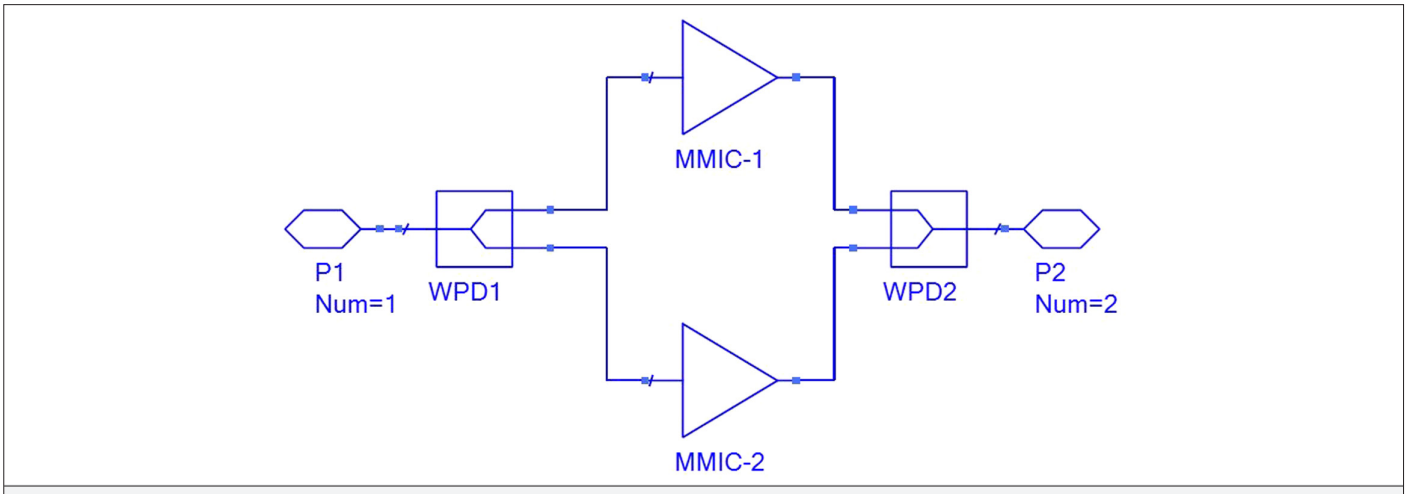

Fig. 2. Block diagram of the proposed HPA.

eliminate the unwanted oscillations, respectively. In the design, the stabilization of the MMIC HPA was achieved with the utilized parallel RC circuit (R1, R2, R3, R4, C7, and C17) at the RF input ports of the transistors. Connection of resistor and capacitor in parallel at the side of gates of HEMTs has been subsidiary to design more stable HPAs. On the other hand, the RC stabilization network also enhanced the gain flatness of the design. Moreover, the μ-factor was aimed to be greater than 1 up to 20 GHz to ensure the unconditional stability condition of the circuit. Meanwhile, IMN and OMN were constructed with respect to the determined optimum load and source impedances, and I/O ports of the HPA were matched to 50 Ω. C3, C4, C5, C8, C9, and C15 capacitors, and TL1, TL2, TL3, TL4, TL5, TL6, TL7, TL8, TL9, TL10, TL11, and TL12 transmission lines were utilized to design IMN and OMN. Furthermore, the series capacitors were utilized in the matching networks as a DC block capacitor. The dimensions of the active and passive components of the layout design are given in Table I.

IV. RESULTS AND DISCUSSION

In the design, Keysight's commercially available Advanced Design System (ADS) software's Momentum tool, which is utilizing the method of moments (MoM) to discretize the integral equations of the EM fields, was utilized to design the layout and perform 2.5D EM analysis. In the design, a two-way WPD was designed to parallel two identical MMIC HPA to multiply output power by 2. In addition, the conventional WPD was comprised of two quarter-wavelength transmission lines and a 100 Ω isolation resistor between the output port

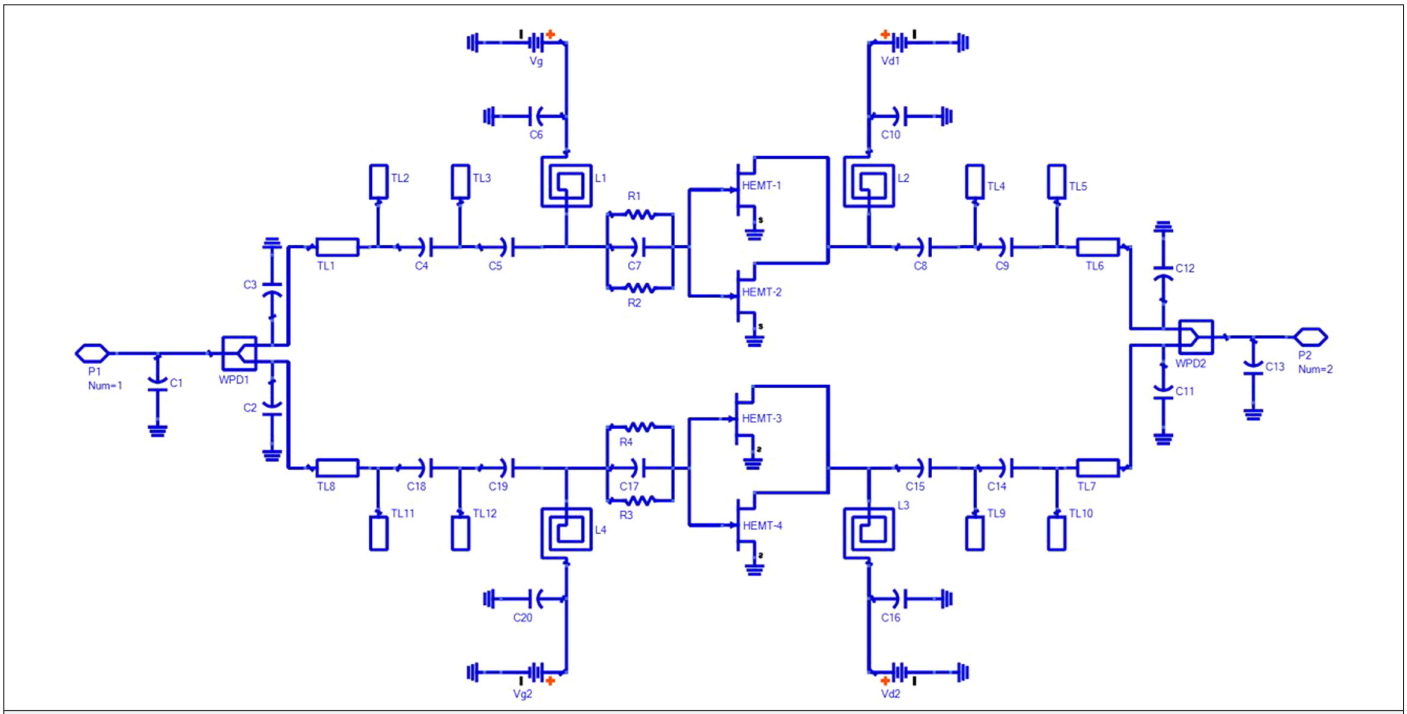

Fig. 3. Schematic view of the proposed HPA.

TABLE I. THE DIMENSIONS OF THE LAYOUT

	W (μm)	L (μm)	Gap (μm)
C1, C13	35	35	24
C2, C3, C11, C12	25	24,7	25
TL_WPD	19	1337	50
R_WPD	39	250	36
TL1, TL8	40	229	20
TL2, TL11	20	629	30
C4, C18	40	47	15
TL3, TL12	40	386	18
C5, C19	98	100	15
L1, L4	35	2,5 turn	20
C6, C20	115	115	20
R1, R2, R3, R4	10	99	34
C7, C17	64	58	43
L2, L3	36	2,5 turn	20
C10, C16	115	115	20
C8, C15	100	100	20
TL4, TL9	16	850	19
C9, C14	44	48	14
TL5, TL10	20	674	31
TL6, TL7	40	235	20
RF Pads	100	125	50
DC Pads	130	150	32

[22, 23]. However, conventional WPD occupies larger areas in the lower frequencies and increases the manufacturing costs. Due to this fact, the π-type miniaturization technique was utilized to miniaturize the design. In this technique, the quarter-wavelength transmission lines were replaced with its equivalent circuit with shunt capacitors and a transmission line between the capacitors. In addition, the branches of the WPD were matched in phase for avoiding additional mismatch losses and thermal problems. In the simulation results of the miniaturized WPD, it was obtained that the input reflection coefficient (S_{11}) and output reflection coefficients (S_{22} and S_{33}) were better than −15 dB and -20 dB, respectively, in the frequency range from 8.5 GHz to 10.5 GHz. Moreover, the insertion losses (S_{21} and S_{31}) were less than −3.7 dB in the operating frequency bandwidth. Besides, the proposed WPD has a compact size of 6 mm^2. The S-parameter simulation results of the proposed WPD are shown in Fig. 4.

In the design process, a unit transistor was selected and all of the four transistors were biased with the same bias conditions. In the EM simulations, all the unit transistors were biased with gain to source voltage (V_{gs}) and drain voltage (V_{ds}) of −2.4 V and 28 V, respectively, and the total drain current (I_{ds}) was 700 mA, which yields a total power dissipation (P_{DC}) of 19.6 W. In the simulation results, it was

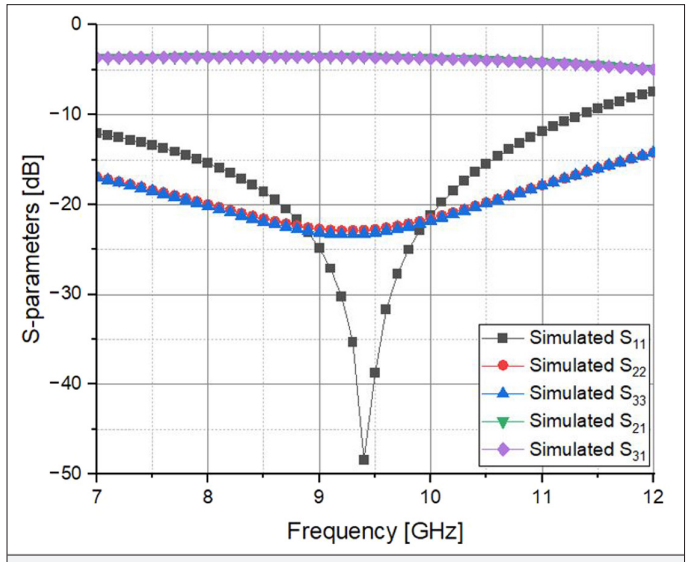

Fig. 4. Simulated S-parameter results of WPD.

observed that $|S_{11}|$ and $|S_{22}|$ were higher than 10 dB while the small signal gain was higher than 10 dB and the fractional bandwidth of the design was observed as 31.58%. The S-parameters simulation results are shown in Fig. 5. Furthermore, the stability analysis of the design was checked according to both μ- and k- stability conditions that are given in Equations 1–3. As a result of the stability analysis, the design was unconditionally stabile up to three times the operating frequency bandwidth. The stability analysis results are shown in Fig. 6.

$$\mu = \frac{1-|S_{11}|^2}{|S_{22}-S_{11}^{*}\Delta|+|S_{21}S_{12}|} > 1 \quad (1)$$

$$k = \frac{1-|S_{11}|^2-|S_{22}|^2+|\Delta|^2}{2|S_{12}S_{21}|} > 1 \quad (2)$$

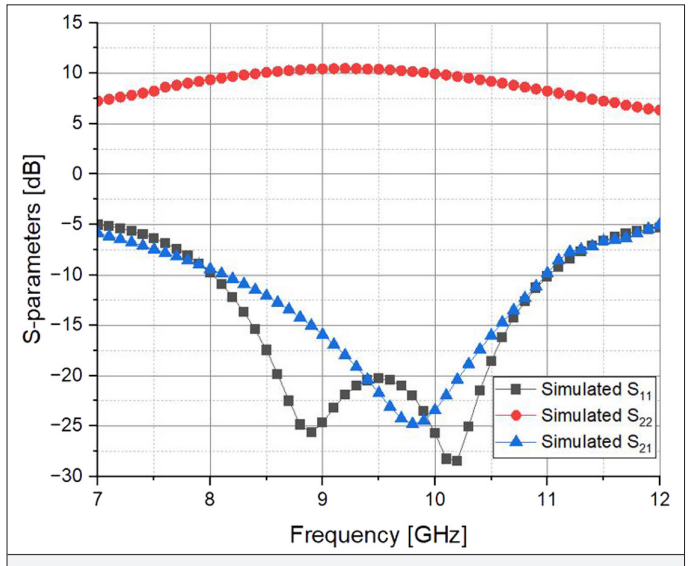

Fig. 5. Simulated S-parameters results of MMIC HPA.

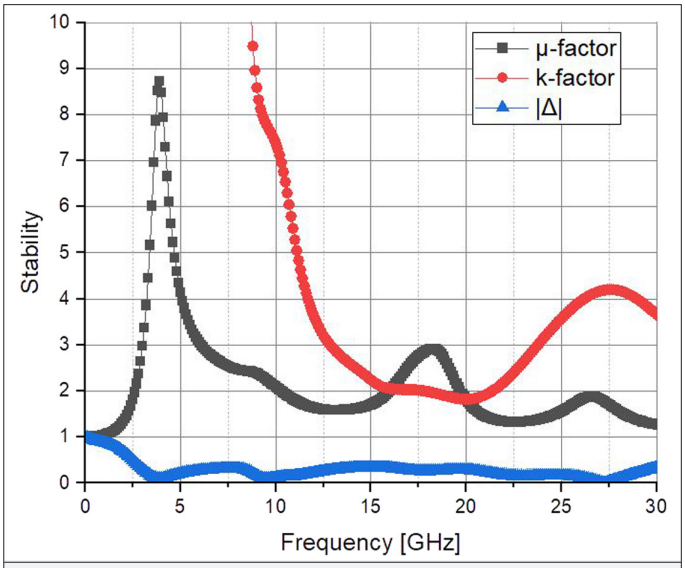

Fig. 6. Simulated stability analysis results of MMIC HPA.

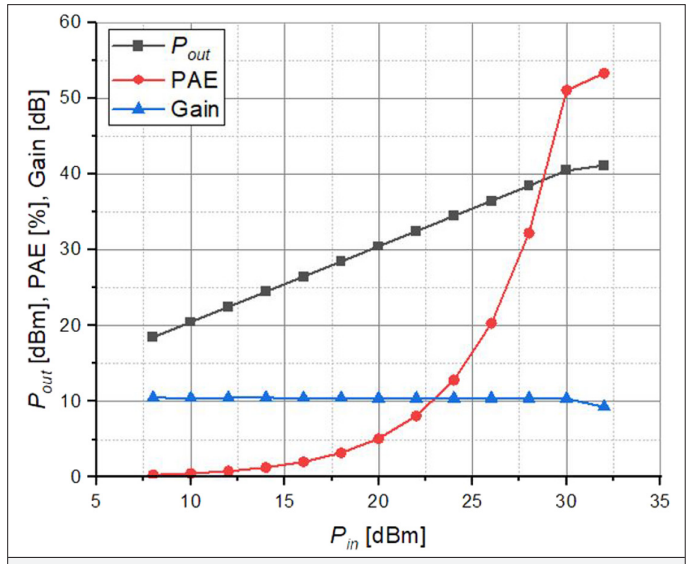

Fig. 7. Simulated large signal parameters results of MMIC HPA.

$$|\Delta| = |S_{11}S_{22} - S_{12}S_{21}| < 1 \quad (3)$$

Moreover, the simulated output power (Pout) was achieved at 41.28 dBm (approximately 13.2 W) when the incident input power (Pin) was 32 dBm and the large signal gain (power gain) was 9.28 dB. The large signal simulation results are shown in Fig. 7. Furthermore, the simulated PAE of the proposed PAE was calculated at approximately 47.34% with respect to (4).

$$PAE = 100.\frac{P_{out} - P_{in}}{P_{DC}}(\%) \quad (4)$$

A layout view of the proposed HPA is shown in Fig. 8, and the dimensions of active and passive components are given in Table I.

As illustrated in Fig. 8, each HEMT has six gates whose structured as γ-shape for increasing available current per mm and breakdown voltage. Therefore, power gain was enhanced [24]. It is important to specify that there are different alternative gate structures such as I-shape, T-shape, π-shape, and so on. It is well-known that types of gate structures are chosen with respect to application specifications that are power added efficiency, gain, maximum available output power, transconductance, threshold voltage, drain-source current density, maximum oscillation frequency (f_{max}), and current gain cut-off (f_t) frequencies [25-27]. Furthermore, it is the rule of thumb that air bridges have been deployed at λ/10 intervals regularly for connecting ground planes properly and eliminating phase differences between ground planes. This is obligatory to get perfect CPW behavior (well-matched) from transmission lines.

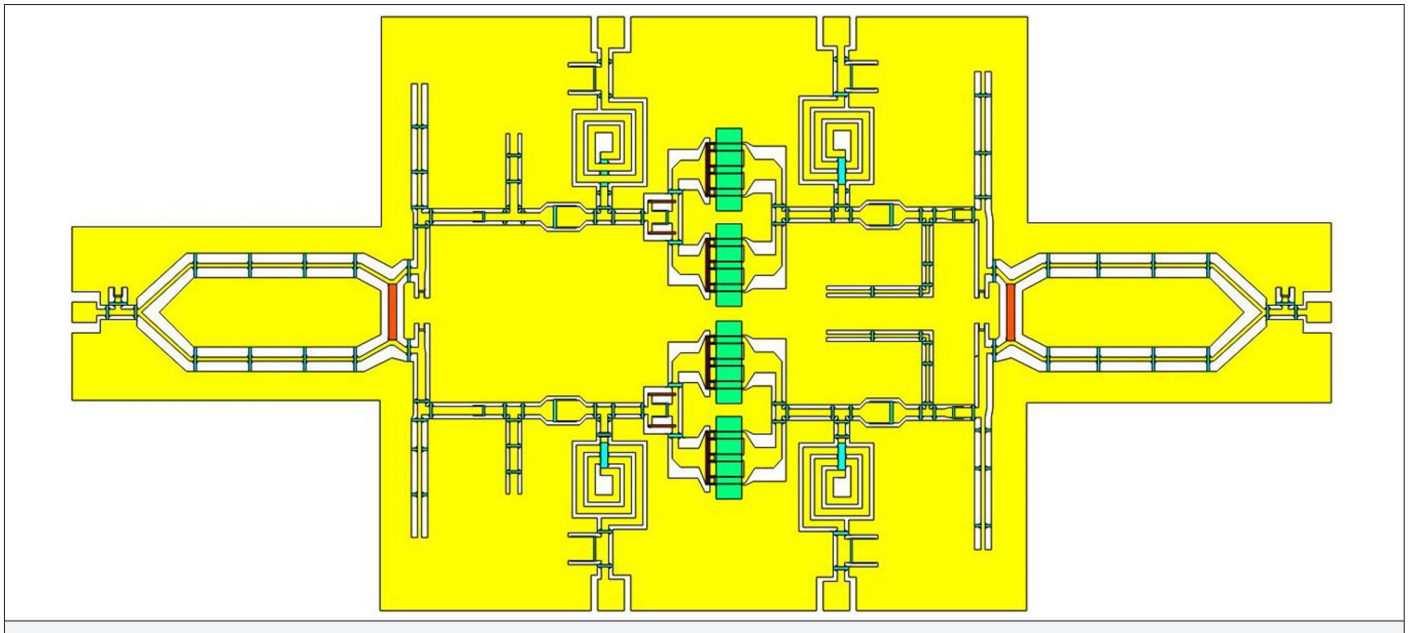

Fig. 8. Layout view of the proposed MMIC HPA.

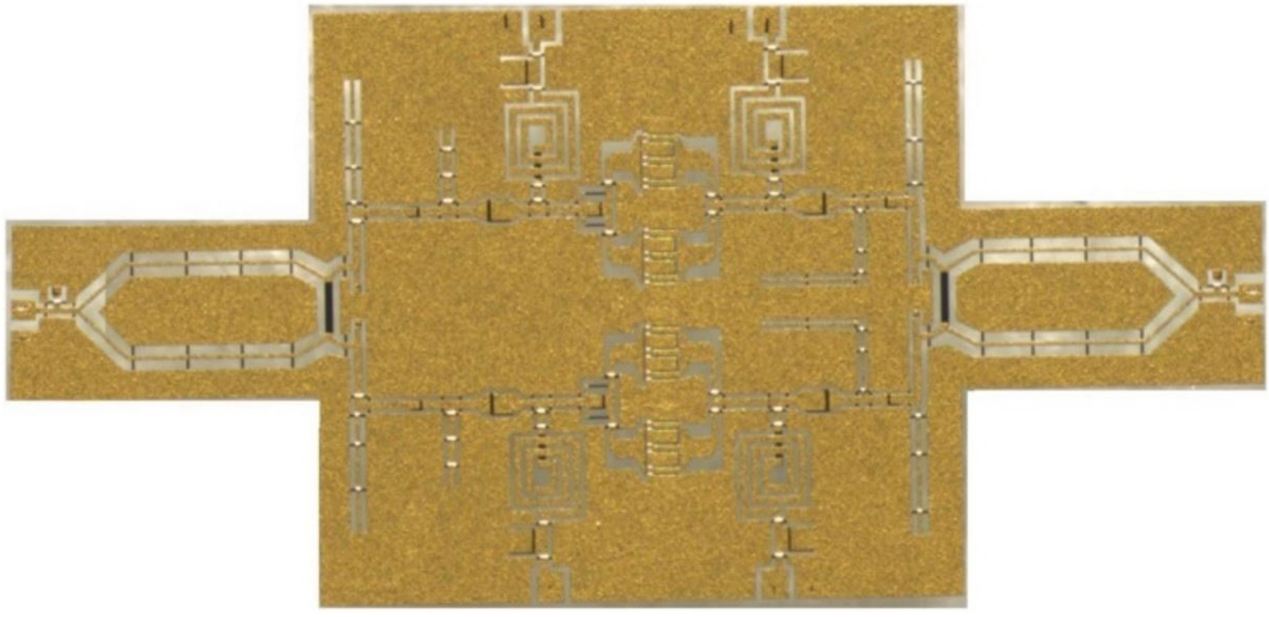

Fig. 9. Microscopic photography of the fabricated MMIC HPA.

The microscopic photography of the fabricated MMIC HPA is presented in Fig. 9 and the total size is 5 mm × 6.5 mm (approximately 0.16 λ × 0.2 λ at 9.5 GHz) excluded WPDs. It should be indicated that each WPD size is 2 mm × 3 mm.

The on-wafer measurements were carried out to validate the simulation results by utilizing the measurement setup that is compromised of The Keysight N5222B PNA, Cascade EPC150RF-LT (up to 67 GHz) manual microwave probe station, and Formfactor I40-A-GSG-150 Infinity RF Probes. Before the measurement, on-wafer short open load thru (SOLT) calibration was performed by utilizing Cascade Microtech ISS model 101–190C calibration substrate. Additionally, V_{gs} and V_{ds} were supplied by utilizing a DC multi-contact wedge probe which is manufactured by GGB Industries Inc., and bias-tee modules were also utilized on the DC supply path.

In the measurement, V_{gs} and V_{ds} were supplied as −2.34 V and 28.02 V, respectively, to obtain similar conditions with the simulations. During measurements, the RF bias procedure was followed. In this type (normally ON), transistors were turned off by applying a negative voltage at the gate side lower than pinch-off voltage. Then, V_{ds} is applied to the drain side and V_{gs} was brought closer to 0 up to read quiescent current (I_{dq}) as same as I_{ds} that had been applied in simulations. Finally, the RF signal was executed. In addition, in the S-parameter measurements, it was observed that the small signal gain exceeds 10 dB roughly for 2 GHz bandwidth. Moreover, $|S_{11}|$ and $|S_{22}|$ were better than 10 dB in the 8.5–10.5 GHz which yields a fractional bandwidth of 21.05%. The comparisons of the simulated and measured S-parameters are shown in Fig. 10.

The large signal measurement was performed at the center frequency of 9.5 GHz at room temperature (25°C). In the large signal characterization, the total drain current (I_{ds}) was equal to 726 mA when 31 dBm input RF power was applied. It is denoted that the consumed DC power that was utilized to calculate PAE equals 20.34 W. Pout of MMIC HPA was obtained as 40.06 dBm (approximately 10.14 W) under 1-dB compression point. From (4), the measured PAE was calculated approximately as 44.53%. Additionally, the large signal gain (power gain) was 9.06 dB. The comparison of the simulated and measured P_{out}, PAE, and gain is shown in Fig. 11.

Table II shows the detailed performance comparison of the MMIC PA in the literature for X-band applications. It is clear that this study has a higher PAE with respect to other studies in the literature, and although output power has decreased with increasing PAE, the proposed work has good output power capability by comparison to its PAE performance [28-32].

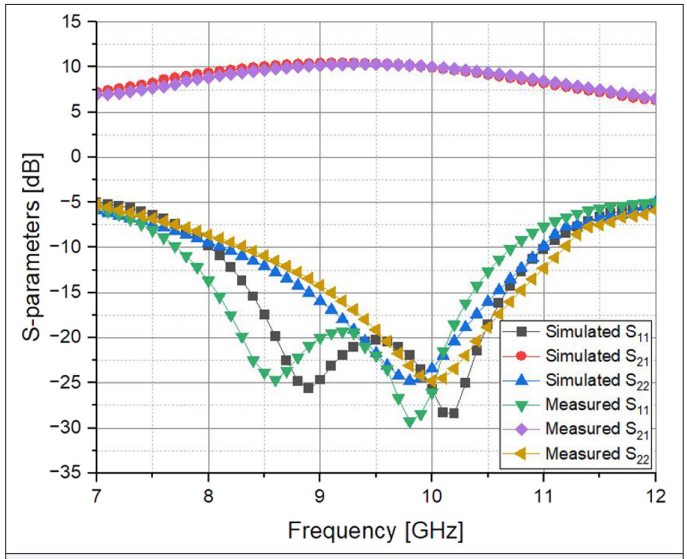

Fig. 10. Comparison of simulated and measured S-parameters results.

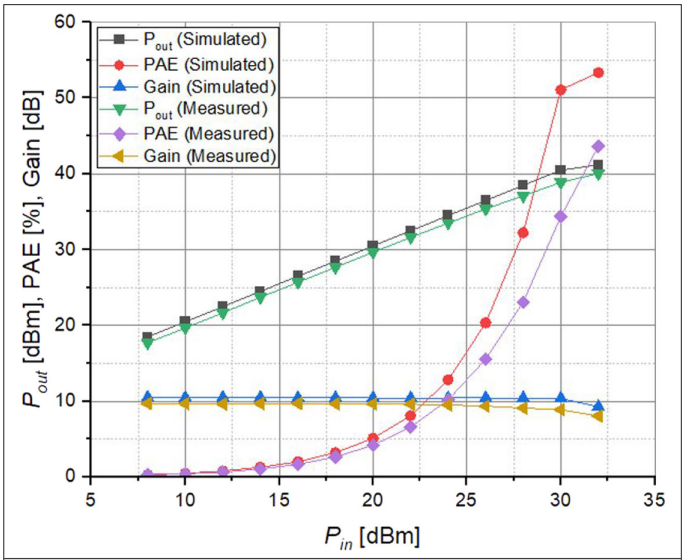

Fig. 11. Comparison of simulated and measured large signal parameters results.

TABLE II. THE COMPARISON TABLE OF X-BAND MMIC PA

Ref.	PAE (%)	P_{out} (dBm)	Bandwidth	V_{ds} (V)
[28]	27	41	2 GHz	25
[29]	38	41.5	1.6 GHz	26
[30]	37.3	42.5	2 GHz	30
[31]	38.6	39.5	3 GHz	30
[32]	71	35.2	N/A	30
[33]	42	42	8.5–9.5	28
[34]	22	31	10–12	28
This work	44.5	40	2 GHz	28

V. CONCLUSION

In this article, a novel X-band MMIC HPA utilizing GaN on SiC technology was presented with a comparison of measurement and simulation results. The HPA achieved a PAE of 44.53% with an output power of 40 dBm in the frequency range from 8.5 GHz to 10.5 GHz. The slight difference between measurement and simulation results could be from unwanted mismatch losses, thermal cooling problems, manufacturing tolerances, and measurement uncertainties. In addition, each wafer could show different electrical characteristics such as photosensitivity, and the thickness of layers such as metals, resistive, and capacitive materials can be altered fabrication by fabrication as a course of its nature. Finally, because of low power consumption, high efficiency, high output power, compact size, and wide operating frequency bandwidth, the proposed device is well suited for AESA radars and could be a direct candidate for communication, electronic warfare, and satellite applications.

Availability of Data and Materials: The data that support the findings of this study are available on request from the corresponding author.

Peer-review: Externally peer-reviewed.

Author Contributions: Concept – G.O.A.; Design – G.O.A.; Supervision – G.O.A.; Resources – G.O.A., B.A.Y.; Materials – G.O.A., B.A.Y.; Data Collection and/or Processing – G.O.A.; Analysis and/or Interpretation – G.O.A.; Literature Search – G.O.A., B.A.Y.; Writing – G.O.A., B.A.Y.; Critical Review – G.O.A.

Declaration of Interests: The authors have no conflict of interest to declare.

Funding: The authors declare that this study has received no financial support.

REFERENCES

1. A. D. Brown, *Active Electronically Scanned Arrays: Fundamentals and Applications*. Chennai, India: John Wiley & Sons, Inc., 2022. [CrossRef]
2. M. D'Urso, M. G. Labate, and A. Buonanno, "Reducing the number of amplitude controls in radar phased arrays," *IEEE Trans. Antennas Propag.*, vol. 58, no. 9, pp. 3060–3064. [CrossRef]
3. D. Han, A. Ogale, S. Li, Y. Li, and B. Sarlioglu, "Efficiency characterization and thermal study of GaN based 1 kW inverter," in IEEE Applied Power Electronics Conference and Exposition-APEC, vol. 2014, 2014, pp. 2344–2350. [CrossRef]
4. S. Chen, "Unlocking the potential of gallium nitride (GaN) for third-generation semiconductors: Advantages, applications, and future prospects," *Highlights Sci. Eng. Technol.*, vol. 81, pp. 342–349, 2024. [CrossRef]
5. G. Longobardi, "GaN for power devices: Benefits, applications, and normally-off technologies," in 2017 International Semiconductor Conference (CAS), Sinaia, Romania, 2017, pp. 11–18. [CrossRef]
6. T. Huang, O. Axelsson, J. Bergsten, M. Thorsell, and N. Rorsman, "Impact of AlGaN/GaN interface and passivation on the robustness of low-noise amplifiers," *IEEE Trans. Electron Devices*, vol. 67, no.: 6, pp. 2297–2303. [CrossRef]
7. P. Kordoš *et al.*, "Influence of gate-leakage current on drain current collapse of unpassivated GaN/ AlGaN/ GaN high electron mobility transistors, (2005)," *Appl. Phys. Lett.*, vol. 86, no. 25, p. 253511, 2005. [CrossRef]
8. H. Lin *et al.*, "Filtenna-filter-filtenna-based FSS with simultaneous wide passband and wide out-of-band rejection using multiple-mode resonators," *IEEE Trans. Antennas Propag.*, vol. 71, no.: 6, pp. 5046–5056, 2023. [CrossRef]
9. J. Yun, S. Trinh-Van, J. Y. Park, Y. Yang, K. Y. Lee, and K. C. Hwang, "Cavity-backed patch filtenna for harmonic suppression," *IEEE Access*, vol. 8, pp. 221580–221589, 2020. [CrossRef]
10. G. R. S. Reddy, and A. Bharathi, "Successive Detection Logarithmic Amplifier for ECCM features of RADAR," in 3rd International Conference on Intelligent Technologies, Hubli, India, 2023, pp. 1–6. [CrossRef]
11. T. Huang, Y. Liu, H. Meng, and X. Wang, "Adaptive waveform design in random stepped frequency radar," in IET International Radar Conference, Xi'an, 2023, pp. 1–5. [CrossRef]
12. M. K. Rao, R. Doerner, S. A. Chevtchenko, S. Haque, and M. Rudolph, "Common-gate LNA MMIC with switching feature using GaN-HEMT for 5G RF front-end," *IEEE Microw. Wireless Tech. Lett.*, vol. 33, no. 10, pp. 1446–1449, 2023. [CrossRef]
13. P. Chen *et al.*, "An optimization method for load modulation trajectories in a millimeter-wave GaN MMIC Doherty power amplifier design," *IEEE Trans. Circuits Syst. II*, vol. 71, no. 1, pp. 141–145, 2023. [CrossRef]
14. B. Cimbili, C. Friesicke, F. van Raay, S. Wagner, M. Bao, and R. Quay, "2.6- and 4-W E-band GaN power amplifiers with a peak efficiency of 22% and 15.3%," *IEEE Microw. Wireless Tech. Lett.*, vol. 33, no. 6, pp. 847–850, 2023. [CrossRef]
15. Y. F. Tsao, P. H. Chiu, S. Chevtchenko, I. Ostermay, J. Würfl, and H. T. Hsu, "Highly robust GaN power amplifier at millimeter-wave frequencies using sputtered iridium gate MMIC technology," *IEEE Trans. Electron Devices*, vol. 70, no. 12, pp. 6244–6249, 2023. [CrossRef]
16. T. Gong *et al.*, "A two-stage high-gain 10-W capacitively coupled distributed amplifier using a new design method," *IEEE Microw. Wireless Tech. Lett.*, vol. 34, no. 5, pp. 520–523, 2024. [CrossRef]
17. R. Nikandish, "GaN integrated circuit power amplifiers: Developments and prospects," *IEEE J. Microw.*, vol. 3, no. 1, pp. 441–452, 2022. [CrossRef]
18. G. Lv, W. Chen, X. Chen, F. M. Ghannouchi, and Z. Feng, "A fully integrated 47.6% fractional bandwidth GaN MMIC distributed efficient power amplifier with modified input matching and power splitting network,"

IEEE Trans. Microw. Theor. Tech., vol. 69, no. 6, pp. 3132–3145, 2021. [CrossRef]
19. M. Zaid *et al.*, "Optimizing low noise amplifiers: A two-stage approach for improved noise figure and stability," *IEEE Access*, vol. 12, pp. 53475–53484, 2024. [CrossRef]
20. R. Sun, J. Lai, W. Chen, and B. Zhang, "GaN power integration for high frequency and high efficiency power applications: A review," *IEEE Access*, vol. 8, pp. 15529–15542, 2020. [CrossRef]
21. M. Kimura *et al.*, "An X-band high power tile-type GaN TR module for low-profile AESA," In IEEE MTT-S International Microwave Symposium (IMS), vol. 2021, 2021, pp. 835–838. [CrossRef]
22. G. O. Arican, "Design and fabrication of compact Wilkinson power divider on gallium nitride coplanar technology," *Mühendislik Bilimleri Derg.* Niğde Ömer Halisdemir Üniversitesi, vol. 12, no. 1, pp. 113–118, 2023. [CrossRef]
23. G. O. Arican, "A compact 2-way multisection power divider for broadband operations," *Sci. Rep.-C*, vol. 2, pp. 1, 2021.
24. C. Wang, R. K. Maharjan, S. -J. Cho, and N. -Y. Kim, "A novel manufacturing process of AlGaN/GaN HEMT for X-band high-power application on Si (111) substrate," *Asia Pacific Microwave Conference Proceedings, Kaohsiung, Taiwan*, vol. 2012, pp. 484–486, 2012. [CrossRef]
25. E. C. Panzo, J. Candido, N. G. Júnior, E. Simoen, and M. G. C. Andrade, "Characterization of AlGaN/GaN HEMTs with different manufacturing characteristics," 38th Symposium on Microelectronics Technology and Devices (SBMicro), Joao Pessoa, Brazil, vol. 2024, 2024, pp. 1–4. [CrossRef]
26. V. V. Painter, R. Sommet, J. -C. Nallatamby, and P. V. Raja, "Influence of field plate, gate width, and voltage dependence of thermal resistance (R_{TH}) for AlGaN/GaN HEMT," *IEEE Trans. Electron Devices*, pp. 1–8, 2024. [CrossRef]
27. P. Pal, and S. Kabra, "Linearity performance and distortion characteristics of T and π – Gate AlGaN/GaN HEMT," Second International Conference on Inventive Computing and Informatics (ICICI), Bangalore, India, 2024, pp. 726–731. [CrossRef]
28. A. Barigelli *et al.*, "Development of GaN based MMIC for next generation x-Band space SAR T/R module," 7th European Microwave Integrated Circuit Conference, Amsterdam, Netherlands, vol. 2012, 2012, pp. 369–372.
29. D. Resca, A. Raffo, S. Di Falco, F. Scappaviva, V. Vadalà, and G. Vannini, "X-band GaN power amplifier for future generation SAR systems," in *IEEE Microw. Wirel. Compon. Lett.*, vol. 24, no. 4, pp. 266–268, 2014. [CrossRef]
30. Y. S. Noh, and I. B. Yom, "A 16 watt X-band GaN high power amplifier MMIC for phased array applications," IEEE International Conference on Microwave and Millimeter Wave Technology (ICMMT), Beijing, China, vol. 2016, 2016, pp. 979–981. [CrossRef]
31. S. Masuda *et al.*, "GaN single-chip transceiver frontend MMIC for X-band applications," *IEEE MTT-S Int. Microw. Symp. Dig., Montreal, QC, Canada*, vol. 2012, pp. 1–3, 2012. [CrossRef]
32. M. Litchfield, M. Roberg, and Z. Popović, "A MMIC/hybrid high-efficiency X-band power amplifier," IEEE Topical Conference on Power Amplifiers for Wireless and Radio Applications. TX, USA: Austin, 2013, pp. 10–12. [CrossRef]
33. S. Vardhan, D. Pathak, M. Mendhe, and A. Dutta, "15W hybrid GaN power amplifier through microstrip radial stub 4W GaN MMIC for X-band radar applications," *IEEE VLSI Device Circuit and System (VLSI DSC)*, pp. 1–5, 2020. [CrossRef]
34. L. Kang, W. Chen, and A. Wu, "A reconfigurable S-/X-band GaN MMIC power amplifier," *IEEE Microw. Wirel. Compon. Lett.*, vol. 32, no. 6, pp. 547–550, 2022. [CrossRef]

Galip Orkun Arican (Member, IEEE) received the B.S. degree from Bilkent University, in 2010, the M.S. degree from Middle East Technical University, in 2014, and the Ph.D. degree from Gazi University, in 2021. From 2010 to 2015, he was a RF MMIC Design Engineer in the Nanotechnology Research Center, Bilkent University. Since 2015, he has been working as a RF/ Microwave Design Engineer in the Directorate of Satellite and Space Technologies of ASELSAN Inc. In addition, he is responsible of developing space qualified communication equipments for satellite payloads such as Receiver, Down-converter, Transmitter, LNA hybrid module, waveguide filter, coupler etc. for LEO/GEO satellite applications. His research interests include high frequency applications, GaN/GaAs MMICs (from C- to W-band), hybrid modules (from C- to Ka-bands), satellite communication payloads, microstrip antennas, filters, waveguides and electromagnetic theory.

Burak Alptug Yilmaz (Member, IEEE) received the B.S. and M.S. degree from Bilkent University, in 2014 and in 2016, respectively. He is currently a Ph.D. candidate in Gazi University. From 2014 to 2016, he was a RF MMIC Design Engineer in the Nanotechnology Research Center, Bilkent University. Since 2016, he has been a RF/Microwave and Antenna Design Engineer in ASELSAN Inc. His research interests include high frequency applications, GaN/GaAs MMICs and RF circuit design (from C- to Ku-band), Active/passive RF devices (multilayer PCBs and modules), phased array antennas, radomes (Land, Naval & Aerospace platforms), Radar and Electronic Warfare Systems, SATCOM Systems (K/Ka-bands).